Direct metal deposition melt pool temperature distribution control through novel holographic beam shaping, allowing improved mechanical and corrosion properties

Matthew Gibson, John Tyrer, and Rebecca Higginson

Citation: ICALEO **2009**, 545 (2009); doi: 10.2351/1.5061608
View online: https://doi.org/10.2351/1.5061608
View Table of Contents: https://lia.scitation.org/toc/ica/2009/1
Published by the Laser Institute of America

DIRECT METAL DEPOSITION MELT POOL TEMPERATURE DISTRIBUTION CONTROL THROUGH NOVEL HOLOGRAPHIC BEAM SHAPING, ALLOWING IMPROVED MECHANICAL AND CORROSION PROPERTIES

Paper 1205

Matthew Gibson[1] John Tyrer[1] Rebecca Higginson[2]
[1]Wolfson School of Mechanical and Manufacturing Engineering, Loughborough University, Loughborough, UK
[2]Department of Materials, Loughborough University, Loughborough, UK

Abstract

When a laser beam is scanned a temperature profile is induced in the workpiece. The temperature distribution will be a function of the beam shape and intensity profile. The use of a circular beam leads to an uneven temperature distribution even when a top hat profile is used. This is caused by the material on the centreline of the beam getting irradiated for longer than an area towards the edge. The uneven temperature distribution will lead to a difference across the weld or deposition in terms of the temperature reached and the rate of cooling. Typically the weld will see a slower cooling rate and maximum temperature along the centreline. This leads to large columnar crystal growth, similar to a cast microstructure with an associated reduction in mechanical performance. A novel method for controlling time-temperature distribution in the material is through the use of a Holographic Optical Element (HOE). The HOE is a computer generated kinoform diffraction pattern that redistributes the beam intensity and shape into any customer designed profile. Through the use of a predictive non-linear thermal model the desired temperature distribution throughout the interaction region was input, and then propagated to the surface. This surface temperature profile was then converted to be the output of the kinoform beam shaping algorithm. This beam shape forms a complex and non intuitive beam profile allowing a controlled time-temperature profile, that can only be achieved in this way. The weld deposition process has been analysed using colour high speed video and optical pyrometry based techniques. This has shown the levels of material transport in the melt pool to be drastically reduced by the DOE redesign of the input beam shape. This is indicative of a reduced thermal gradient in the melt pool, leading to greater control of the deposition microstructure.

Introduction

Laser cladding uses the energy of a laser beam to fuse a material addition to the surface of a component. This material can be different to the bulk component to alter the surface properties of the part, or of a similar material to enable repair of a worn or damaged component. Laser cladding emerged as a process following the introduction of high power CO_2 lasers in the late 1970's. Firstly as a pre-placed powder process [1] and shortly after as a blown powder technique in 1983 by Weerasinghe and Steen [2].

Material transport in the deposition melt pool is mainly driven by the temperature gradient present. This will drive buoyancy and viscous flows, shaping the profile of the deposition. In the case of a Gaussian beam intensity distribution the high intensity at the centre of the beam induces a melt pool with a thermal gradient from the centre out. This thermal gradient will drive surface flow from the centre out to the edges of the deposition, which will then be fed by an internal buoyancy flow rising up the centre of the weld pool. This material transport will have a contributing effect on the doming of the deposition, resulting in the need to overlap tracks to achieve a uniform deposition, as shown in Figure 1.

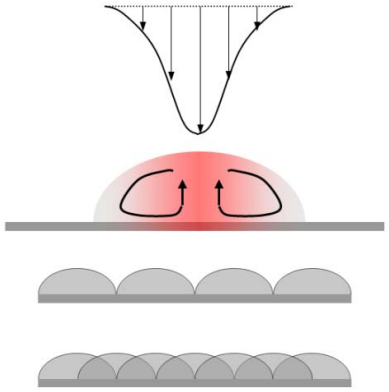

Figure 1: Schematic diagram of material transport and need for overlap in Gaussian beam deposition

Observations of the material transport at the surface of the deposition melt pool can be used as a tell tale to an understanding of the temperature gradients

present in the pool. The temperature gradient in the melt pool will have a controlling effect on the formation of the microstructure, with a strong gradient leading to differential cooling rates and therefore crystal growth. By modifying the heat input to the deposition, influence can be gained over the temperature gradients present. The modified melt pool flow will have an effect to reduce doming of the depositions, leading to reduced overlap between tracks and improved surfaces. Reducing thermal gradients will also serve to even cooling rates, providing a greater consistency in microstructure.

This study looks at how the melt pool surface flow has been altered by redistributing the beam intensity flux. A novel method of redistributing a high power beam is the use of Diffractive Optical Elements (DOE). A DOE is a reflective array of pixels whose surfaces are stepped sub wavelength levels. When a coherent beam reflects from the element surface the output beam is a series of wavefronts, one from each pixel. At a reconstruction plane the out of phase beams have undergone constructive and destructive interference and form a pre-determined beam profile. The optical element also provide a focusing function to the beam allowing control of beam shape, intensity distribution and size in a single element. The DOE's used are a complex computer generated diffraction pattern known as a Kinoform, and exhibit a diffraction efficiency of >90%. DOE's have been used successfully in a number of fields, Hardening [3,4], multiple point soldering, simultaneous cutting and welding of polymers [4]. And conduction welding [5-7].

High speed video has been used to record the flow at the surface of the melt pool. Optical pyrometry has been used in many fields for the visualisation of combustion temperatures [8,9]. This investigation used similar processing techniques to visualise the surface flow fields. By scaling the video frames to the red channel the intensity information is removed from the signal, leaving only colour information. Changes in the colour of the deposition pool can be related to the temperature and emissivity at a specific point. By tracking how the areas of differing colour move over the surface information on the speed and direction of flow can be obtained.

Experimental Procedures

Depositions were made of Inconel 625 powder onto a substrate of 1.5mm mild steel. The substrates were laser cut into discrete sections to allow multiple welds to be made on each substrate without residual heat conducting through the substrate affecting later depositions. To remove the influence of injected powder mass flow profiles the powder was pre-placed onto the substrate. Prior to spreading of the deposition material the substrate was cleaned with Isopropanol alcohol.

All depositions were made using a Coherent S48 slow flow CO_2 laser producing a maximum output of 1.2kW, with all power measurements taken on an internal power meter. A slow flow laser has been chosen to provide a stable output beam profile. The laser is fitted with a twin optical setup. A conventional refractive cutting head is fitted, giving a Gaussian or TEM_{00} beam, or the laser can be used to illuminate the DOE mirror to provide custom beam outputs. The work piece was set at different depths below the focal point of the cutting head to give a beam diameter matching the width of the customised beam. The beam widths were matched by making burns into Perspex. The work piece was traversed beneath the beam using an Anorad CNC-2000 two axis table. All depositions were made using air as a shield gas, the role of the gas was only to keep the optical elements free from debris and fume.

The depositions were made using two customised beam profile referred to as Half Pipe and Half Pipe Wedge. A graphical representation of the profile is given in Figure 2, along with the TEM00 profile used as a comparison. The Half Pipe profiles are scanned parallel to the trough axis.

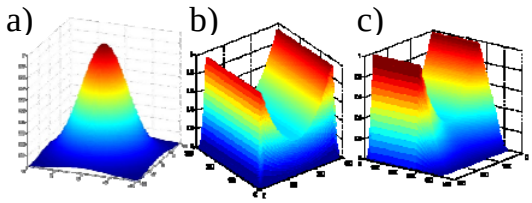

Figure 2: Beam irradiance distribution of a) TEM_{00} beam, b) Half Pipe Wedge and c) Half Pipe.

Thermal modelling has shown the thermal propagation of the different beam profiles without melting. As can be seen from Figure 3, the Half Pipe beam irradiance distribution provides a more consistent heating across the irradiated region, showing a flatter bottom surface to the isotherms shown. When this heating pattern is applied to the molten deposition pool it is expected the uniform heating provided will reduce mass transport effects contributing to the doming of the deposition surface.

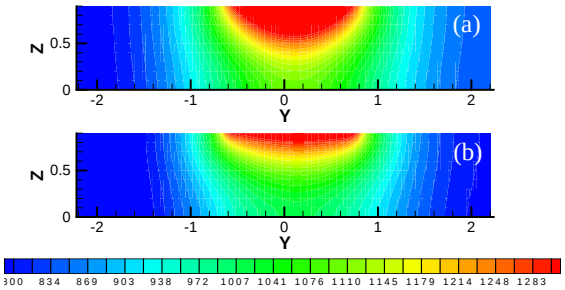

Figure 3: Thermal propagation of (a) TEM00 and (b) Half Pipe beam profiles

High Speed Video

Depositions were made and imaged with an Olympus iSpeed 3 colour camera system. All videos were taken at 1500fps. The camera position is fixed relative to the laser head looking along the axis of the work piece traverse, shown in Figure 4. This allows a static view of the deposition forming relative to the laser beam. The deposition process can be seen under external lighting conditions in Figure 5.

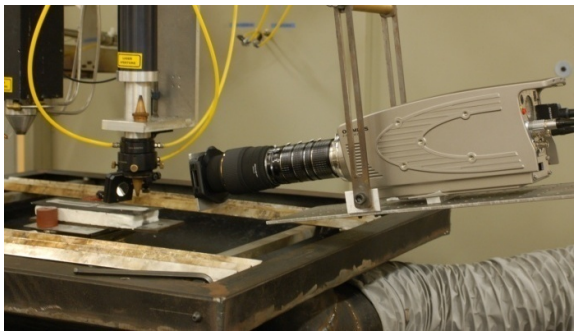

Figure 4: High speed camera set up to film DOE beam deposition

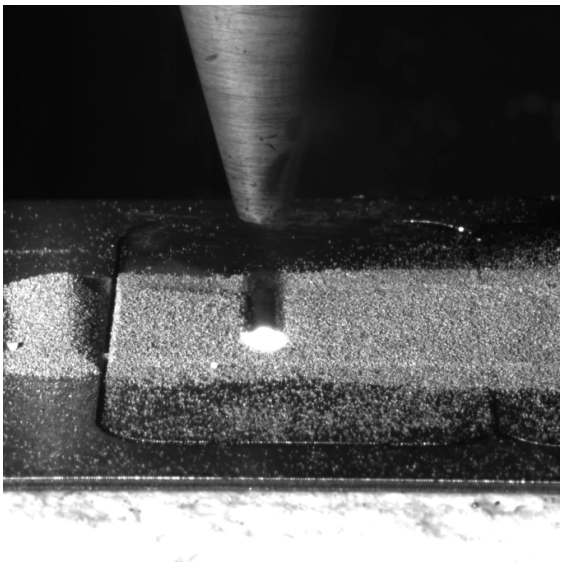

Figure 5: Low magnification frame of deposition using a cutting head under lit conditions showing the camera view.

The videos use the self illumination of the molten weld pool, with a infra red blocking filter in place to protect the camera CCD. The iSpeed 3 camera uses a Bayern filter arrangement to get red, green and blue signals on one sensor, with a built in algorithm to convert the signal from each pixel on the sensor into a RGB value for each pixel in the image. The camera was used to output an uncompressed bitmap image for each frame.

Results and Discussion

High Speed Video

Videos of depositions made with the parameters in Table 1 have been taken. The diameter of the Gaussian beam has been expanded to 2mm, this gives all the depositions the same nominal width. Differing parameters are needed for the beam distributions, this is due to the abilities of the shapes to initiate melting of the materials. The high intensity "spike" in the center of the Gaussian beam means this distribution is able to induce melting at a lower power and higher speed.

Table 1: Laser parameters for high speed videoed depositions

	TEM_{00}	Half Pipe	Half Pipe Wedge
Beam Size (mm)	2Ø	2 x 2	2x3
Powder Track Thickness (mm)	0.5	0.5	0.5
Power (W)	750	850	1000
Traverse Speed (mm/s)	5	3.5	3

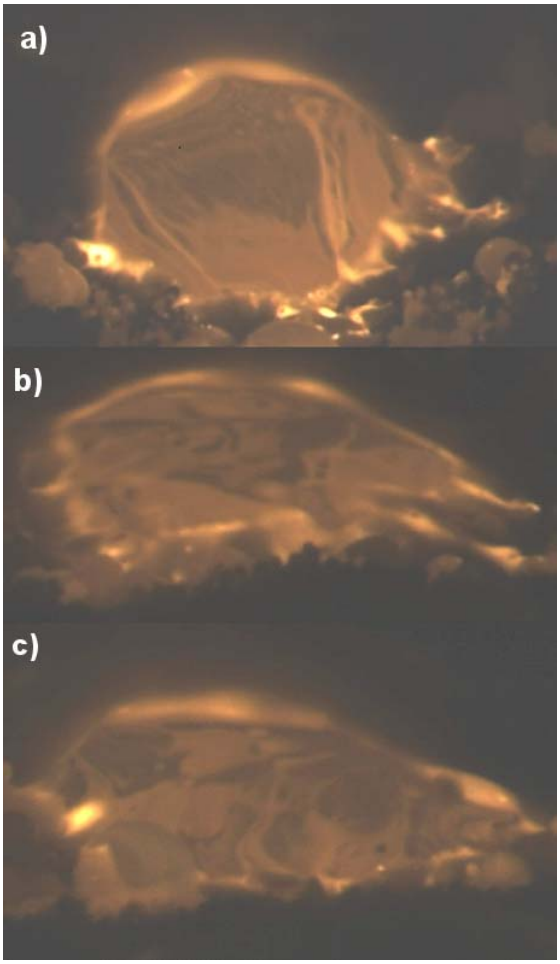

Figure 6: Screenshots of the deposition melt pools for a) Gaussian, b) Half Pipe and c) Half Pipe Wedge beam intensity distributions

Screen shots of the deposition melt pool from the three different beam profiles are shown in Figure 6. The shape of the melt pools is different for the three beam intensity distributions. The image of the melt pool formed by the Gaussian beam intensity distribution shows a circular leading and trailing edges. The melt pools for the two Half Pipe beam distributions are much squarer at both leading and trailing edges. It is thought this is a combination of the shape of the melt pool induced by the circular beam distribution along with a doming to the surface of the Gaussian melt pool caused by the flow of material within the pool.

To aid visualization of the surface of the deposition pool, the intensity component of the image has been removed. This has been achieved by scaling the RGB value for each pixel to achieve the ratio between the red, green and blue levels. This results in an image with only the colour information remaining. Colourmap screenshots of the deposition pools are shown in Figure 7.

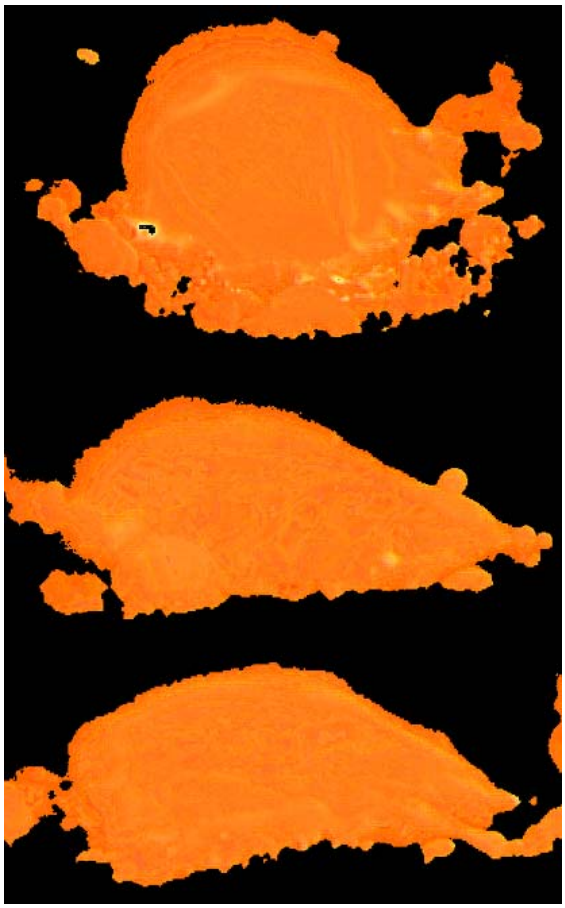

Figure 7: Colour map images of the three beam distributions, a) Gaussian, b) Half Pipe and c) Half Pipe Wedge.

For a clearer view of the stirring action at the surface of the weld pool, a greyscale image of the ratio between two colour channels has been calculated. In this case the ratio between the red and blue signals. The greater the intensity in the image the hotter the object it originated from. As the hotter the object, the shorter the wavelength of light emitted will be. This

gives a greater proportion of blue light reaching the camera's sensor.

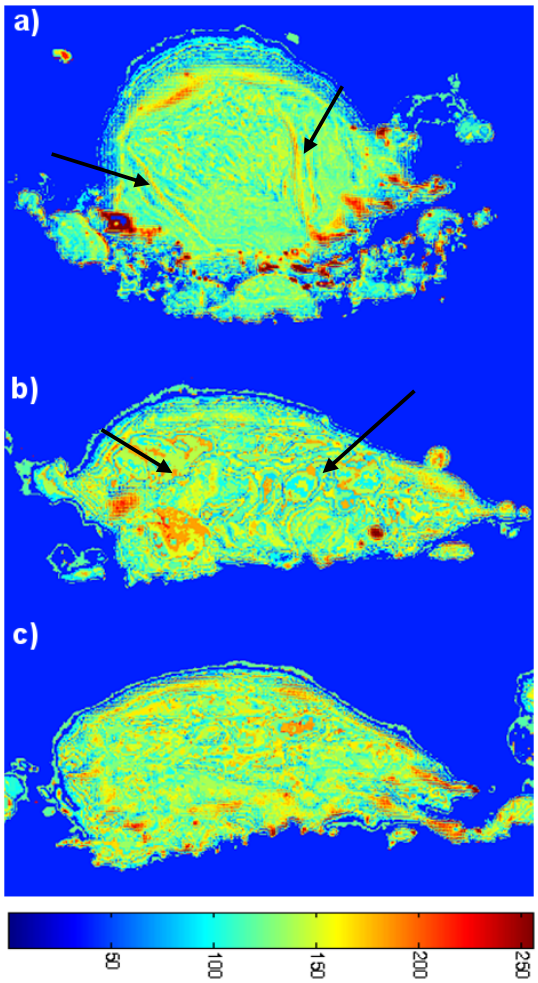

Figure 8: Frames at 1ms intervals showing the stirring action within melt pools, a) Gaussian, b) Half Pipe and c) Half Pipe Wedge.

The still frames in Figure 8 indicate different flows on the surface of the melt pools. The Gaussian induced melt pool shows a laminar flow from the centre of the leading edge over the sides of the pool. In the image two flow lines are visible, indicated by arrows. Both the Half Pipe melt pools show more turbulent flow regimes, with eddy like formations on the surface, these are indicated with arrows on the image of the Half Pipe melt pool.

Table 2: Surface mass transport flow velocities for different beam intensity distributions

Beam Distribution	Minimum Velocity	Maximum Velocity	Mean Velocity
Gaussian	0.311	0.607	0.422
Half Pipe	0.005	0.024	0.016
Half Pipe Wedge	0.006	0.020	0.013

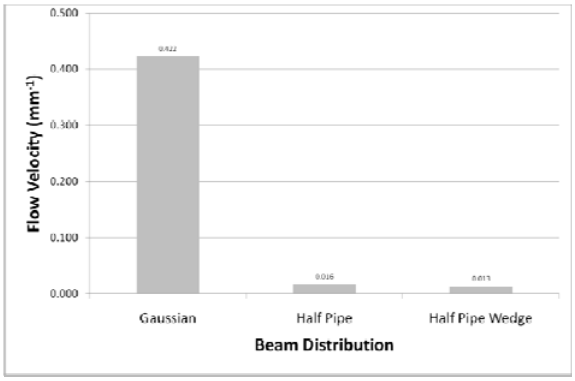

Figure 9: Histogram showing the mean flow velocities for the three intensity distributions

Image analysis software ImagePro Plus v6 has been used to run traces on the flow at the surface of the deposition pools. Using the time interval between frames of 666µs and dimensions gained by imaging a scale marker with the high speed camera system the velocity of the surface flow can be obtained. The data in Table 2 and Figure 9 show the velocities for the surface flow in the three deposition pools. As can be seen in the figure the velocity of in the Gaussian melt pool is far greater than either of the Half Pipe distributions. An approximate 20 times reduction in the velocity is seen between the Gaussian distribution and the plain Half Pipe, and a further 1.3 times reduction with the Half Pipe Wedge. In addition to the decrease in velocity the flow appears to be more random, with little overall direction. A schematic of the observed flow patterns is given in Figure 10. Flow in the Gaussian melt pool is seen to originate from a region at the centre of the leading edge of the pool, with some material taken over and out from the weld pool centre, A stronger flow is seen running around the sides of the melt pool close to the bottom edge. It is thought that the flow mechanism is strong enough not to allow the regions of differing colour observed to flow over the melt pool, instead having to flow round the sides. In contrast the flow in the half pipe distributions was seen to be originating from the whole width of the leading edge, and flowing up onto the top surface of

the melt pool. In this region a degree of turbulent flow was observed with little overriding direction, only a slow flow across to the rear of the pool. this follows the expected outcome, where the greater uniformity in heating has reduced the driving force for the flow, and therefore removed directionality and velocity.

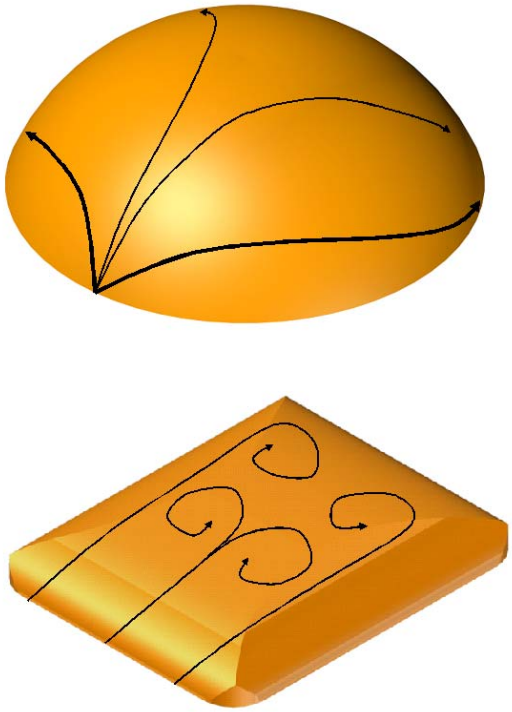

Figure 10: Schematic of the observed flow patterns

With the preplaced powder method used in this investigation it was observed that material was being melted forward of the leading edge of the melt pool, Figure 11 shows a frame from the video showing such a case. When this material reaches the leading edge of the weld, it is mixed into the main melt pool, where the sudden mass addition has a destabilising effect the pool. The leading wedge to the Half Pipe Wedge distribution has served to preheat the deposition, removing the formation of the volumes of material, and smoothing the addition of material into the melt pool. It is anticipated that this is the reason for the reduction in the velocity of the melt pool flow.

Figure 11: Frame from Half Pipe distribution melt pool showing molten material forward of pool leading edge

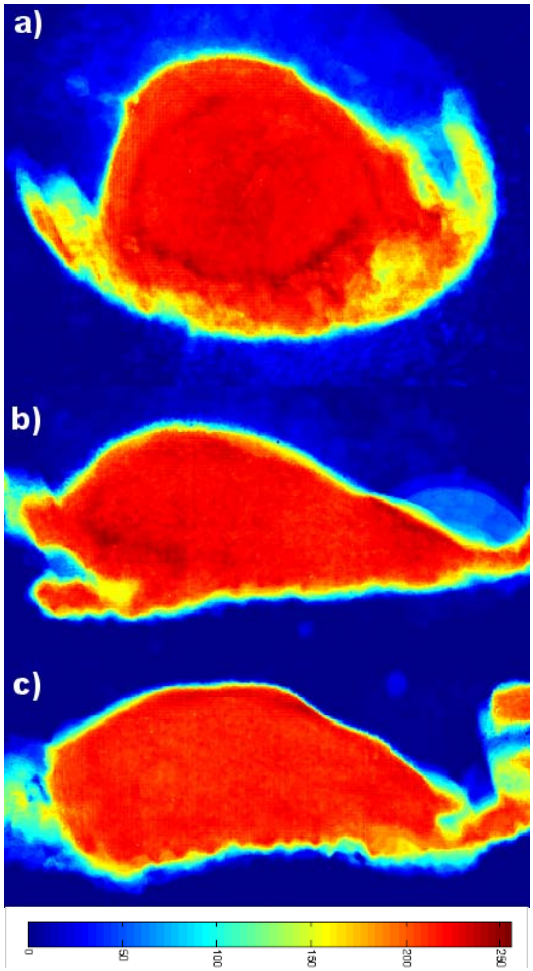

Figure 12: Relative total intensity at each pixel over 100 frames, a) Gaussian, b) Half Pipe and c) Half Pipe Wedge.

The rapid turbulent stirring seen in the half pipe depositions, makes visualisation of any overall mechanism difficult. The summing of the individual values for the intensity of the red-blue ratio at each pixel over a number of frames will indicate if there is an overriding mechanism driving regions of heat and

flow at each pixel. The resulting pseudo-colour images are shown in Figure 12. The Gaussian distribution melt pool shows a greater intensity in the centre of the melt pool. This is due to the increased intensity at the centre of the Gaussian beam inducing a higher temperature in this region of the melt pool. In the Gaussian distribution melt pool a ring of high intensity is visible in the melt pool, this is thought to be regions of heated Inconel 625 or oxide being driven round the melt pool by the flow observed following this pattern. The total intensity image for the half pipe distribution is showing hotter regions along the side edges of the melt pool, this is thought to be due to the extra intensity of the half pipe in these regions. The totalled image for the Half Pipe Wedge intensity distribution shows a uniform intensity, this therefore shows an even level of heat at the surface of the deposition.

Conclusions

This study has taken three different beam intensity distributions and shown that the velocity and type of weld pool flow has varied between them.

The deposition melt pool induced by the Gaussian beam profile has shown to be circular in shape and domed in profile, this is due to the shape and intensity of the Gaussian beam, the melt pool formed by the HOEs are both rectangular in shape and are seen in the video frames to have a flatter top surface. This is due the reconstructed intensity profiles modifying the temperature gradient and therefore the forces shaping the melt pool.

By separating the intensity component of the video frames from the colour component a clearer view of the surface patterning can be made. This has allowed the visualisation of flow features on the surface, the Gaussian deposition pool shows flow lines across the surface where rapid laminar movement of the surface texture is seen. With both the Half Pipe distributions the surface movement appears to by more turbulent, with less overall directionality.

By calibrating the images in ImagePro software the velocity of surface flow can be measured, this was shown to be 20 times slower in the Half Pipe distribution then the Gaussian.

Relative thermal profiles of the deposition surface have been achieved, this has shown the centre of the Gaussian deposition to be of an elevated temperature, along with a region around the melt pool, where it is believed the surface flow is present. The preheating wedge added to the Half Pipe distribution has served to stabilise the mass addition to the melt pool, allowing uniform heating of the melt pool.

Acknowledgements

The authors would thank Olympus Industrial for the use of the iSpeed 3 camera system and assistance in setup. Also John Jones of Laser Optical Engineering Ltd for the thermal modelling of beam profiles used, Sara Noden and Daniel Lloyd also of Laser Optical Engineering for calculation and manufacture of the Diffractive Optical Elements.

References

[1] Belmondo A, Castagna M. Wear-resistant coatings by laser processing. Thin Solid Films 1979;64.

[2] Weerasinghe VM, Steen WM. Laser Cladding With Pneumatic Powder Delivery. 1983:166.

[3] Leung MKH, Man HC, Yu JK. Theoretical and experimental studies on laser transformation hardening of steel by customized beam. International Journal of Heat and Mass Transfer, 2007 11;50(23-24):4600-4606.

[4] Noden SC. The application of diffractive optical elements in high power laser materials processing. PhD Thesis, Loughborough University, UK, 2000.

[5] Kell J. Melt Pool and Microstructure Manipulation Using Diffractive Holographic Elements in High Power Conduction Laser Welding. 2007.

[6] Kell J, Tyrer J, Higginson R, Thomson T, Jones J, Noden S. Holographic diffractive optical elements allow improvements in conduction laser welding of steels. ICALEO 2006 Congress Proceedings; LMP Conference 2006; 99:8-17.

[7] Kell J, Tyrer J. R., Higginson R.L., Thomson R.C. Microstructural characterization of autogenous laser welds on 316L stainless steel using EBSD and EDS. J.Microsc. 2005;217(2):167-173.

[8] Lu G, Yan Y. Temperature profiling of pulverized coal flames using multicolor pyrometric and digital imaging techniques. IEEE Transactions on Instrumentation and Measurement 2006;55(4):1303-1308.

[9] Panagiotou T, Levendis Y, Delichatsios M. Measurements of particle flame temperatures using three-color optical pyrometry. Combust.Flame 1996;104(3):272-287.